THE JOURNAL OF BIOLOGICAL CHEMISTRY VOL. 284, NO. 38, pp. 25973–25983, September 18, 2009

Demonstration of Proton-coupled Electron Transfer in the Copper-containing Nitrite Reductases*[S]

Received for publication, April 23, 2009, and in revised form, June 5, 2009 Published, JBC Papers in Press, July 7, 2009, DOI 10.1074/jbc.M109.012245

Sibylle Brenner[‡], Derren J. Heyes[‡], Sam Hay[‡], Michael A. Hough[§], Robert R. Eady[§], S. Samar Hasnain[§1], and Nigel S. Scrutton[‡2]

From the [‡]Manchester Interdisciplinary Biocentre and Faculty of Life Sciences, University of Manchester, Manchester M1 7DN and the [§]Molecular Biophysics Group, School of Biological Sciences, University of Liverpool, Liverpool L69 7ZB, United Kingdom

The reduction of nitrite (NO_2^-) into nitric oxide (NO), catalyzed by nitrite reductase, is an important reaction in the denitrification pathway. In this study, the catalytic mechanism of the copper-containing nitrite reductase from *Alcaligenes xylosoxidans* (*Ax*NiR) has been studied using single and multiple turnover experiments at pH 7.0 and is shown to involve two protons. A novel steady-state assay was developed, in which deoxyhemoglobin was employed as an NO scavenger. A moderate solvent kinetic isotope effect (SKIE) of 1.3 ± 0.1 indicated the involvement of one protonation to the rate-limiting catalytic step. Laser photoexcitation experiments have been used to obtain single turnover data in H_2O and D_2O, which report on steps kinetically linked to inter-copper electron transfer (ET). In the absence of nitrite, a normal SKIE of ~1.33 ± 0.05 was obtained, suggesting a protonation event that is kinetically linked to ET in substrate-free *Ax*NiR. A nitrite titration gave a normal hyperbolic behavior for the deuterated sample. However, in H_2O an unusual decrease in rate was observed at low nitrite concentrations followed by a subsequent acceleration in rate at nitrite concentrations of >10 mM. As a consequence, the observed ET process was faster in D_2O than in H_2O above 0.1 mM nitrite, resulting in an inverted SKIE, which featured a significant dependence on the substrate concentration with a minimum value of ~0.61 ± 0.02 between 3 and 10 mM. Our work provides the first experimental demonstration of proton-coupled electron transfer in both the resting and substrate-bound *Ax*NiR, and two protons were found to be involved in turnover.

Denitrification is an anaerobic respiration pathway found in bacteria, archaea, and fungi, in which ATP synthesis is coupled to the sequential reduction of nitrate (NO_3^-) and nitrite (NO_2^-) ($NO_3^- \rightarrow NO_2^- \rightarrow NO \rightarrow N_2O \rightarrow N_2$) (1–3).[3] The first committed step in this reaction cascade is the formation of gaseous NO by nitrite reductase (NiR), the key enzyme of this pathway. Two distinct classes of periplasmic NiR are found in denitrifying bacteria, one containing cd_1 hemes as prosthetic groups (4–6) and the other utilizing two copper centers to catalyze the one-electron reduction of nitrite (7). Copper-containing NiRs are divided into two main groups according to the color of their oxidized type 1 copper center (T1Cu), with shades ranging from blue to green (3, 7). NiR from *Alcaligenes xylosoxidans* subsp. *xylosoxidans* (NCIMB 11015, *Ax*NiR), which is analyzed in this study, is a member of the blue CuNiR group. The blue and green subclasses show a high degree of sequence similarity (70%) (8) and have similar trimeric structures with each monomer (~36.5 kDa in *Ax*NiR) consisting of two greek key β-barrel cupredoxin-like motifs as well as one long and two short α-helical regions (7, 9).

Each NiR monomer contains two copper-binding sites per catalytic unit. One is a T1Cu center, which receives electrons from a physiological redox partner protein and is buried 7 Å beneath the protein surface (10), and the other copper is a type 2 center (T2Cu), constituting the catalytically active substrate-binding site (11). The physiological electron donor for the blue NiRs are the small copper protein azurin (14 kDa) (7) and cytochrome c_{551} (7, 12, 13). The T1Cu, which is responsible for the color of NiR, serves as the electron delivery center and is coordinated by two histidine residues as well as one cysteine and one methionine residue. The catalytic T2Cu, which like all T2Cu centers has very weak optical bands, is ligated to three His residues and an H_2O/OH^- ligand in the resting state. This H_2O/OH^- ligand is held in place by hydrogen bonds to the active site residues, Asp-92 (*Ax*NiR numbering) and His-249, and gets displaced by the substrate during catalytic turnover (14). The T2Cu is located at the base of a 13–14-Å substrate access channel at the interface of two monomers with one of the three His residues being part of the adjacent subunit (15, 16). The two copper centers are connected by a 12.6-Å covalent bridge provided by the T1Cu-coordinating Cys and by one of the T2Cu His ligands (17, 18). This linkage has been suggested to constitute the electron transfer (ET) pathway from the T1Cu center to the catalytically active T2Cu center via 11 covalent bonds (19).

Intramolecular ET from T1- to T2Cu has been extensively examined using pulse radiolysis studies (7, 19–24). In a variety

* This work was supported by TgK Scientific Ltd. (Ph.D. studentship to S. B.) and by Biotechnology and Biological Sciences Research Council Project Grants BB/D016290/1 (to S. S. H.) and BB/G005850/1 (to N. S. S.).

[S] The on-line version of this article (available at http://www.jbc.org) contains supplemental text, additional references, Table S1, and Figs. S1–S8.

[1] To whom correspondence may be addressed. Tel.: 44-151-795-5149; E-mail: s.s.hasnain@liverpool.ac.uk.

[2] Biotechnology and Biological Sciences Research Council Professorial Research Fellow. To whom correspondence may be addressed: Tel.: 44-0161-306-5152; E-mail: nigel.scrutton@manchester.ac.uk.

[3] The abbreviations used are: NO, nitric oxide; NiR, nitrite reductase; *Ax*NiR, nitrite reductase from *Alcaligenes xylosoxidans* subsp. *xylosoxidans* (NCIMB 11015); DT, dithionite; ET, electron transfer; NMN, *N*-methylnicotinamide; PCET, proton-coupled electron transfer; PR, phenol red; PT, proton transfer; SKIE, solvent kinetic isotope effect; T2DNiR, nitrite reductase lacking the copper atom in the T2Cu center; PMS, phenazine methosulfate; MES, 2-(*N*-morpholino)ethanesulfonic acid; AU, absorbance unit.

of NiR species, ET could be measured, both in the presence and absence of substrate, with observed ET rate constants ($k_{ET(obs)}$) ranging from ~150 to ~2000 s^{-1}. According to the Marcus semi-classical ET theory (25), the redox potentials (E'_0, redox midpoint potential at pH 7.0) of the copper centers affect both the thermodynamic equilibrium and the ET kinetics. In the absence of substrate, the difference in the redox potentials has been found to be insignificant at pH 7 (E'_0 (T1Cu) ~240 mV and E'_0 (T2Cu) ~230 mV (20)), implying a thermodynamically equal electron distribution between the two metal centers. From an enzymatic point of view, however, approaching this equilibrium position on such a fast time scale (≥150 s^{-1}) is unfavorable in the absence of substrate, as NiR has been shown to form an inactive species with a reduced T2Cu that is devoid of the H_2O/OH^- ligand and unable to bind nitrite (26, 27). Substrate binding has been proposed to induce a favorable shift in the T2Cu redox potential, which would be expected to result in an accelerated ET compared with the substrate-free reaction (7, 16, 25, 27–30). However, $k_{ET(obs)}$ values in *Axg*NiR (GIFU1051) have been demonstrated to be lower in the nitrite-bound than in the substrate-free enzyme between pH 7.7 and 5.5 (21). Below pH 5.5, the ET rate constants were observed to be similar in the nitrite-free and -bound enzyme (21).

In addition to changes in the redox potentials and thus in the driving force of the ET reaction, several structural changes in the redox centers have been reported as a result of substrate binding, which may also influence the inter-copper ET rate by changing the reorganization energy (16, 25, 30, 31). These rearrangements include subtle changes in the Cys-His bridge linking T1- and T2Cu (32) and conformational transitions of the catalytically relevant active site residue Asp-92 (see below and Ref. 29). Moreover, the presence of nitrite has been postulated to be relayed to the T1Cu site via the so-called substrate sensor loop (via His-94, Asp-92, and His-89 in *Ax*NiR), thereby triggering ET to the T2Cu (19, 27, 29, 32). The tight coupling of ET to the presence of substrate has been argued to prevent the formation of a deactivated enzyme species with a prematurely reduced T2Cu (14, 16, 19, 26, 27, 33). In accordance with such a feedback mechanism, in a combined crystallographic and single-crystal spectroscopic study, inter-copper ET could only be detected in crystals where nitrite was bound to the T2Cu site, whereas in the absence of substrate no such ET was observed (34). This finding, however, contradicts the pulse radiolysis results at room temperature (see above), and the apparent discrepancy between solution studies and x-ray crystallographic data collected at cryogenic temperature remains to be resolved.

The one-electron reduction of nitrite to NO involves two protons according to the chemical net equation $NO_2^- + 2H^+ + e^- \rightarrow NO + H_2O$, if the T2Cu is ligated by an H_2O molecule in the resting state rather than an OH^- ion. Although the exact enzymatic mechanism is still somewhat controversial (35, 36), one suggested reaction sequence is given in Scheme 1. The potential participation of active site residues in catalyzing the proton transfer (PT) steps has been investigated by studying the pH dependence of NiR under steady-state conditions as well as by pulse radiolysis. The trends obtained for k_{cat} and $k_{ET(obs)}$, are similar with pH optima between 5.2 and 6, indicating the involvement of two amino acid residues (21, 22, 37).

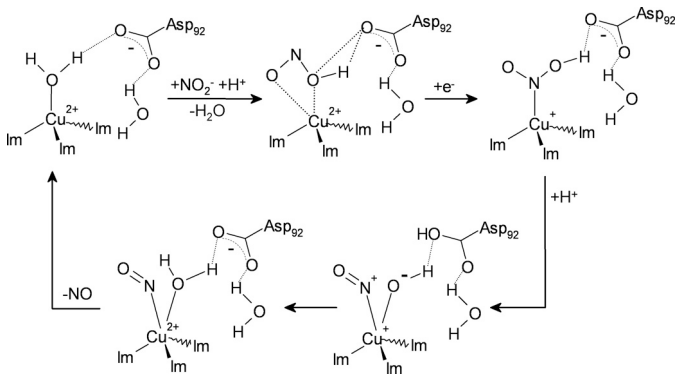

SCHEME 1. **A potential reaction mechanism proposed for CuNiRs.** Adapted from Ref. 36. Nitrite is shown to bind to the oxidized T2Cu as nitrous acid, thus involving the first protonation step. It coordinates to the oxidized T2Cu center in a bidentate fashion. Following inter-copper ET yielding a reduced T2Cu center, the initially deprotonated Asp-92 accepts a proton, which is subsequently transferred to the substrate. His-249 may be a potential source of this second proton. PT and ET reactions may be reversible and they may be concerted rather than sequential as suggested by the *arrows*. See text for further information.

Asp-92 and His-249 have been proposed as acid-base catalysts (18, 21, 22, 28, 38), and the abrupt drop in rates at increasing pH may indicate that OH^- can act as a competitive inhibitor for nitrite (39). The relevance of these active site residues, however, as well as the timing of the two protonation steps is still a matter of debate (35, 40, 41).[4]

There are no experimental studies that have been aimed at directly examining the kinetic coupling of PT and ET steps in *Ax*NiR. In this study of the blue *Ax*NiR, our aims were to gain further insight into the mechanism of nitrite reduction by combining multiple turnover experiments with laser photoexcitation studies to measure the (single turnover) inter-copper ET. An extensive analysis of the solvent kinetic isotope effect (SKIE) has been employed as a means of determining whether solvent-exchangeable protons and/or water molecules play a rate-limiting role in the catalytic turnover and/or in inter-copper ET.

MATERIALS AND METHODS

Reagents—NADH was purchased from Melford Laboratories (Suffolk, UK). Luria-Bertani medium was from ForMedium (Norfolk, UK). NaCl, KCl, Tris, di-potassium hydrogen phosphate, and potassium di-hydrogen phosphate were from Fisher. D_2O was from Goss Scientific Instruments Ltd. (Essex, UK). Kanamycin, isopropyl thiogalactoside, KNO_2, $CuSO_4$, DNase, lysozyme, MES, dithionite, phenol red (PR), ascorbate, phenazine methosulfate (PMS), bovine methemoglobin. and *N*-methylnicotinamide (NMN) were purchased from Sigma.

NiR Purification—Recombinant NiR from *A. xylosoxidans* subsp. *xylosoxidans* (NCIMB 11015, *Ax*NiR) was overexpressed in *Escherichia coli* BL21(DE3) cells, and the purification was similar to the method described previously (42, 43) (see supplemental material for detailed description). *Ax*NiR concentrations were determined using an extinction coefficient of

[4] Very recently spectroscopic and computational methods have shown that ET from the T1 to the T2Cu sites in the green copper enzyme *Rs*NiR (*Rhodobacter sphaeroides*) requires the initial proton transfer from the Asp residue in the active site pocket to nitrite thereby triggering the reductive cleavage of the substrate (40, 41).

ϵ_{595} = 6.3 mM^{-1} cm^{-1} (9, 18). The *Ax*NiR enzyme lacking the copper atom in the T2Cu center (T2DNiR) was expressed and purified in the same way as *Ax*NiR except that the dialysis steps into $CuSO_4$ were omitted (27, 42, 44).

Anaerobic Experimental Conditions and Sample Preparation—All experiments were conducted in a Belle Technology glovebox under a nitrogen atmosphere except for the laser photoexcitation measurements, for which samples were prepared in the glovebox, transferred into rubber-sealed quartz cuvettes, and taken out of the box. Buffers were made anaerobic by bubbling with nitrogen for at least 20 min and transferred into the glovebox; the bottles were then left open overnight to achieve complete equilibration with the anaerobic atmosphere. Oxygen levels were kept below 5 ppm throughout the experiment. Enzyme solutions were made oxygen-free by passing through a PD-10 column (GE Healthcare) pre-equilibrated with the anaerobic buffer.

Multiple Turnover Phenol Red Experiments—Multiple turnover experiments using the pH indicator PR were performed in unbuffered solution (110 mM KCl, distilled H_2O) with an ionic strength equivalent to 50 mM potassium phosphate (KP_i), pH 7.0. The reaction was observed in a Cary UV-50 Bio UV-visible scanning spectrophotometer (Varian Inc.) using a 1-mm path length cuvette to allow the use of higher dye concentrations. The initial PR spectrum was adjusted to match the spectrum obtained in buffered solution at pH 7.0 ($AU_{432}/AU_{556} \cong 2$). The $[H^+]$-dependent absorbance change of the PR spectrum was used to monitor the protons being taken up during the turnover of *Ax*NiR with its natural substrate nitrite (NO_2^-). The reductant ascorbate in combination with the mediator PMS served as an artificial electron donor system. The sample mixture included 1 μM *Ax*NiR, KNO_2 concentrations between 25 and 160 μM, 300 μM PR, 10 μM PMS, and 1 mM ascorbate. Progress curves were recorded until the thermodynamic equilibrium of the enzymatic reaction was reached and were then corrected for the background reaction of the electron donor with the substrate observed in the absence of enzyme.

Proton calibration curves were obtained by titrating incomplete sample mixtures with defined amounts of hydroxide ions. Three standard curves were produced using 300 μM PR only, 300 μM PR + 1 μM *Ax*NiR, and the complete sample except the substrate. The average curve was used to determine the changes in proton concentration upon multiple turnover of *Ax*NiR.

Steady-state Kinetics of AxNiR—The steady state activity of *Ax*NiR was determined in 50 mM KP_i, pH 7.0 (100% H_2O), and 50 mM KP_i, pH 6.59 (100% D_2O), at 4 °C using deoxyhemoglobin (deoxyHb) as an NO scavenger and observing the spectral changes upon binding of NO to deoxyHb. Bovine hemoglobin was purchased as methemoglobin, reduced by dithionite (DT) in the glovebox, and made anaerobic by passing through a PD-10 column, yielding deoxyhemoglobin. Hb concentrations were determined aerobically using an extinction coefficient for oxyHb of ϵ_{414} = 131 mM^{-1} cm^{-1} per monomer (45).

The steady-state kinetics of *Ax*NiR were measured anaerobically at 430 nm using an Applied Photophysics SC18MV stopped-flow instrument with a 2-mm path length. 30 μM heme (7.5 μM deoxyHb, 15 μM heme after mixing), 10 mM ascorbate (5 mM after mixing), and 100 μM PMS (50 μM after mixing; E'_0 = +92 mV (27, 46)) were mixed with varying KNO_2 concentrations ($[KNO_2]$ = 0.01–50 mM after mixing) and three different *Ax*NiR concentrations ([NiR] = 5, 10, and 20 nM after mixing) for each KNO_2 concentration. The ionic strength was adjusted to $([KNO_2] + [KCl])_{\text{after mixing}}$ = 50 mM.

Progress curves of nitrite reduction by *Ax*NiR were recorded by measuring the absorbance change at 430 nm associated with NO binding to heme. To calculate the steady state activity of *Ax*NiR, initial rates were determined from the slopes of the progress curves using less than 20% of the decreasing ΔAU_{430}. The slopes ($\Delta AU_{430} \cdot s^{-1}$) were corrected for the ΔAU_{430} resulting from the background nitrite reductase activity of deoxyHb. These values were converted into units of micromolars NO·s^{-1} by dividing through a calibration factor of 0.0232 $\Delta AU_{430} \cdot \mu M^{-1}$ obtained in a calibration experiment using limiting KNO_2 concentrations.

To check the validity of the Hb-linked assay, the results were compared with a continuous spectrophotometric assay using DT as reductant and following its depletion at 315 nm (ϵ_{315} = 8 mM^{-1} cm^{-1} (37)). This assay was also conducted in the stopped-flow using 50 mM KP_i, pH 7.0 (100% H_2O), at 4 °C, and an ionic strength of $[KNO_2]$ + [KCl] after mixing = 50 mM. As described for the Hb assay, 2 mM DT and 100 μM PMS were mixed with varying KNO_2 concentrations and three different *Ax*NiR concentrations for each KNO_2 concentration yielding steady-state rates for *Ax*NiR.

Laser Photoexcitation Experiments—Sample solutions with a volume of 750 μl were prepared in a 1-cm path length quartz cuvette and sealed "air-tight" inside the glovebox. Samples contained 30 μM *Ax*NiR, 200 μM NADH as electron donor, 50 mM NMN as mediator, and varying KNO_2 concentrations. The standard buffer system was 50 mM KP_i, pH 7.0, at 4 °C. For proton inventory and SKIE experiments, the pH value was determined using a conventional pH-meter, and the pH reading ($pH_{(obs)}$) was corrected using (47) as shown in Equation 1,

$$pH_{obs} = pH_{desired} - (\Delta pH)_n = pD - (\Delta pH)_n$$
$$= pD - (0.076 \cdot n^2 + 0.3314 \cdot n) \quad \text{(Eq. 1)}$$

where $(\Delta pH)_n$ is a correction factor depending on the volume fraction of D_2O (n), *i.e.* n = 1 for pure D_2O. Proton inventory experiments, in which the amount of D_2O was varied from 0 to 100% (*i.e.* $0 \leq n \leq 1$), were also conducted in KP_i buffer, using the above equation to determine the corrected pH value. The ratio of the rate constants obtained in 100% H_2O (k_{H2O}) and the rate constants in pure (~95%) D_2O (k_{D2O}) gave the SKIE)for the reaction SKIE = k_{H2O}/k_{D2O}.

During laser photoexcitation experiments, the samples were excited at 355 nm using the third harmonic of a Q-switched Nd-YAG laser (Brilliant B, Quantel). The energy output of each laser pulse was 200 mJ, and pulses were 6–8 ns in duration. Spectral transients were collected at 595 nm using an Applied Photophysics LKS-60 flash photolysis instrument with the detection system at right angles to the incident laser beam. Experiments were performed at various temperatures between 4 and 40 °C by using a circulating water bath (Fisher brand). The probe light (150-watt xenon lamp) was passed through a monochromator before and after passage through the sample.

Absorbance changes were monitored using a photomultiplier tube. Kinetic transients were measured over time bases up to 50 ms; samples were excited only once, and triplicate measurements were collected for each condition.

Data Evaluation—All data were analyzed using the software package Origin (OriginLab, Northampton, MA).

The steady-state data for *Ax*NiR were analyzed by the classical Michaelis-Menten Equation 2,

$$\frac{\nu_{obs}}{[E_0]} = \frac{k_{cat} \cdot [KNO_2]}{K_m + [KNO_2]} \quad \text{(Eq. 2)}$$

yielding the catalytic rate constant k_{cat} and the Michaelis-Menten constant K_m. Kinetic traces obtained in the laser experiments were fitted double-exponentially as shown in Equation 3,

$$\Delta AU_{595} = AU_0 + \Delta AU_{1\,(obs)} \cdot \exp(-k_{1(obs)} \cdot t) + \Delta AU_{2(obs)} \cdot \exp(-k_{2(obs)} \cdot t) \quad \text{(Eq. 3)}$$

where $k_{1(obs)}$ and $k_{2(obs)}$ are the observed rate constants, assigned to T1Cu reduction and inter-copper electron transfer, respectively; $\Delta AU_{1(obs)}$ and $\Delta AU_{2(obs)}$ are the corresponding absorbance changes; t is the elapsed time after the flash, and AU_0 is an offset absorbance value. The nonstandard equations used to fit the substrate concentration dependences of the observed rate constants in 95% D_2O (Equation 6), 100% H_2O (Equation 7), and of the SKIE (Equation 8), respectively, are given under "Results and Discussion."

Proton inventory experiments were analyzed by plotting the ratio of the rate constant k_n, obtained at a certain volume fraction of D_2O (n), and the rate constant k_0 in pure H_2O *versus* n. The data were fitted linearly indicating that one proton may be involved in Equation 4 (48):

$$k_n/k_0 = (1 - n - n \cdot p_1) \quad \text{(Eq. 4)}$$

where $p_1 = 1/SKIE$.

The temperature dependences of the observed rate constants were fitted to the Eyring given by Equation 5,

$$\ln(k_{obs} \cdot T^{-1}) = -(\Delta H^{\ddagger}/R) \cdot T^{-1} + (\Delta S^{\ddagger}/R) + \ln(k_B \cdot T^{-1}) \quad \text{(Eq. 5)}$$

where T is the absolute temperature, R the gas constant, and k_B Boltzmann's constant. The activation enthalpy $\Delta H^{\ddagger}$ can be obtained from the slope and the activation entropy $\Delta S^{\ddagger}$ from the y intercept allowing the calculation of the free activation energy $\Delta G^{\ddagger}$.

RESULTS AND DISCUSSION

Proton Consumption upon Multiple Turnover of AxNiR—The number of protons consumed by *Ax*NiR during turnover was measured in unbuffered solution using the pH indicator PR. In a multiple turnover situation one *Ax*NiR molecule catalyzes the production of NO many times, and the proton delivery route within the protein itself is depleted during the first round(s). Thus, to continue catalysis, the enzyme has to replenish its proton pool from the bulk solvent. In the absence of any buffer components the pH indicator will reflect this change in proton concentration directly by changing its acid-base equilibrium and hence the indicator color. Upon consumption of protons the PR spectrum decreases at 432 nm (the acidic, yellow absorbance peak) and increases at 556 nm (the basic, pink peak).

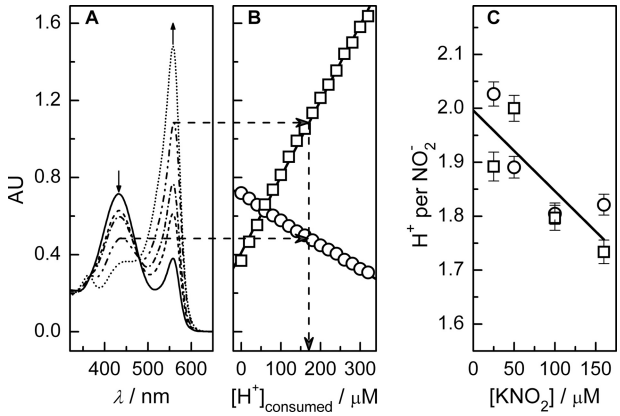

FIGURE 1. **Proton consumption by NiR under multiple turnover conditions using the pH indicator PR.** The *error bars* are smaller than the symbol size if invisible. *A,* final absorbance spectra of PR after NiR has reached the thermodynamic equilibrium of turnover for varying nitrite concentrations (*solid line*, no KNO_2; *dashed*, 25 μM KNO_2; *dash-dot*, 50 μM KNO_2; *dash-dot-dot*, 100 μM KNO_2; *dot*, 160 μM KNO_2). The *small arrows* indicate the absorbance changes upon proton consumption by NiR. *B,* averaged proton calibration curves obtained for the absorbance signals at 432 nm (*circles*) and 556 nm (*squares*) by titrating PR with defined amounts of OH^- (supplemental Fig. S1). *Solid lines* are linear fits. The *dotted arrows* overlapping *A* and *B* exemplify the determination of the proton concentration being consumed by NiR. *C,* protons consumed per nitrite molecule present in the sample mixture at varying nitrite concentrations. *Circles,* 432 nm; *squares,* 556 nm. *Solid line,* linear fit to all data points.

The PR absorbance change was calibrated by adding defined amounts of hydroxide ions to the sample mixture without any enzyme turnover taking place (see supplemental Fig. S1). These standard curves were then used to determine the amount of protons being consumed during the catalytic turnover of *Ax*NiR, in which the enzyme was reacted with a defined amount of substrate (KNO_2) in the presence of an excess of artificial reductant (ascorbate) and mediator (PMS). Spectra were recorded until the monitored absorbance change reached its maximum value (Fig. 1). At low nitrite concentrations ~2 protons were found to be consumed during one catalytic round. Because of the previously demonstrated reversibility of nitrite reduction by NiR (49), this ratio dropped slightly at higher initial substrate concentrations (~1.8 at 160 μM nitrite). To account for the shift in the chemical equilibrium as a function of the initial substrate and thus the final product concentration, all data points shown in Fig. 1*C* were fitted linearly. An extrapolation of the fit to 0 μM KNO_2 gave a y axis intercept of 2.0 ± 0.04. Hence, the PR assay provided the first experimental evidence that two protons are coupled to turnover in NiR.

Steady-state Activity of AxNiR in H_2O and D_2O—The catalytic activity of *Ax*NiR was determined in buffered (50 mM KP_i) H_2O, pH 7.0, and 95% D_2O, pD 7.0, to determine whether there is a measurable SKIE indicative of a proton-coupled process. The steady-state turnover of *Ax*NiR was monitored using a novel assay with the NO scavenger deoxyhemoglobin (deoxyHb) to measure product formation. DeoxyHb shows a significant absorbance change at its heme Soret peak at 430 nm upon binding of NO (supplemental Fig. S2). With reported on-rates for NO binding to deoxyHb of ~2.4×10^7 M^{-1} s^{-1} and

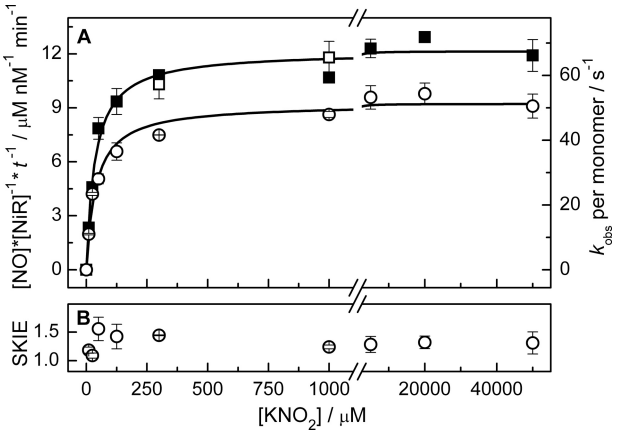

FIGURE 2. **Steady-state assay for NiR using deoxyHb as NO scavenger.** *A*, Michaelis-Menten plot for NiR in 50 mM KP_i at 4 °C using 100% H_2O (pH 7.0, *closed* and *open squares*) and 100% D_2O (pH 6.59, *open circles*) as solvent, respectively. *Solid lines* represent fits to the Michaelis-Menten equation (Equation 2). The *error bars* are smaller than the symbol size if invisible. For the *closed squares* and the *open circles*, progress curves of nitrite reduction were recorded by measuring the absorbance change at 430 nm associated with NO binding to 15 μM heme (supplemental Fig. S3). Initial rates were determined from the slopes using less than 20% of the decreasing ΔAU_{430}. The slopes (ΔAU_{430}·s^{-1}) were corrected for the ΔAU_{430} resulting from the background nitrite reductase activity of deoxyHb and were converted into units of μM NO·s^{-1} using a calibration factor of 0.0232 ± 0.0006 ΔAU_{430}·μM^{-1} (supplemental Fig. S4). Three different NiR concentrations were analyzed for each substrate concentration, which is reflected in the *error bars*. As a control, the *open squares* were measured using dithionite as reductant and monitoring its depletion at 315 nm. *B*, SKIE obtained as the ratio of the observed steady-state rates in H_2O and D_2O at varying substrate concentrations.

cooperative off-rates as small as 4.6×10^{-5} s^{-1} and 2.2×10^{-5} s^{-1} for the α and β chains, respectively (50), this indicator reaction is expected to be a useful reporter for the *Ax*NiR turnover reaction. Moreover, the reaction rate of nitrite with heme proteins has been reported to be 10,000 times smaller than that of NO (51). To ensure steady-state initial rate conditions for *Ax*NiR as well as for NO scavenging, the experiment was performed in a stopped-flow instrument by mixing varying enzyme and substrate concentrations with 15 μM heme, excess reductant (ascorbate) and mediator (PMS). The heme absorption was monitored at 430 nm, and complete progress curves were recorded, *i.e.* data were collected until no further absorbance change was detectable indicative of fully NO-ligated heme (supplemental Fig. S3). Less than 20% of the decreasing trace was analyzed by linear regression, yielding initial rates, which were converted from units of ΔAU_{430}·s^{-1} into units of μM NO·s^{-1} through dividing by a calibration factor (see supplemental Fig. S4 for details).

Michaelis-Menten plots for *Ax*NiR in H_2O and D_2O at 4 °C are presented in Fig. 2 and were fitted to Equation 2. The deoxyHb assay yielded an apparent Michaelis-Menten constant K_m of 36 ± 5 μM in H_2O and of 40 ± 5 μM in D_2O, respectively. The value in H_2O is in accordance with the published K_m of 34 μM determined at pH 7.5 using the electron donor dithionite (37). Furthermore, as a control for the calibration of this new assay, the catalytic activity of NiR was measured using dithionite as reductant and detecting its depletion at 315 nm as described previously (37). The good agreement between the two approaches (Fig. 2) confirmed the validity of the deoxyHb-linked assay for NiR activity described here. This assay has the advantage that only the forward reaction is measured because sequestration of the product NO prevents NiR from catalyzing the reverse reaction. In addition it also prevents the side reaction (catalyzed by NiR) of the reduction of exogenous NO to form N_2O. The k_{cat} value in 100% H_2O was found to be 12.1 ± 0.3 μmol·min^{-1}·$nmol^{-1}$ (110 μmol·min^{-1}·mg^{-1}). Previously published values were determined using a stopped-time assay at room temperature, in which residual nitrite was detected colorimetrically by the use of the Griess reagent. Because of the difference in temperature, the reported k_{cat} values were slightly higher with specific activities of 176 μmol·min^{-1}·mg^{-1} (pH 7.0, 23 °C) (20), 167 μmol·min^{-1}·mg^{-1} (43), and 236 μmol·min^{-1}·mg^{-1} (pH 7.1, 25 °C) (16).

The SKIE determined over the whole substrate concentration range gave moderate values between 1.1 and 1.5 (Fig. 2*B*) indicating a possible contribution of one proton or one solvent molecule to the rate-limiting catalytic step(s). This minor elevation of the SKIE is unlikely to report on both protons/two solvent molecules. In contrast to these results, no SKIE was observed for the green NiR of *Rhodobacter sphaeroides* at pH 6.0 suggesting that the rate-limiting step may change with the pH value and/or may depend on the origin of the enzyme (52).

Single Turnover Kinetics Using Laser Photoexcitation—T1- to T2Cu ET in NiR can be observed upon reducing the T1Cu center by artificial electron donors, as shown previously in pulse radiolysis studies (7, 19–22). Because the T1Cu is located only 6–7 Å below the protein surface (7, 20), it is much more readily reduced than the more buried T2Cu (12–13 Å (16, 17)), resulting in a color change from the blue T1Cu in the oxidized state (Cu(II), $\epsilon_{595} = 6.3$ mM^{-1} cm^{-1}) to colorless in the reduced state (Cu(I), supplemental Fig. S5). Following the initial reduction of the T1Cu, the electrons redistribute between the two copper centers according to the thermodynamic equilibrium, which is determined by the difference in the copper redox potentials (20, 29). Because the contribution of the T2Cu center to the optical absorbance spectrum of *Ax*NiR is negligible in either reduction state (7, 32, 46), monitoring of the inter-copper ET reaction by optical spectroscopy is limited to the T1Cu signal at 595 nm.

All laser experiments were performed in 50 mM KP_i using NADH as an artificial electron donor. Upon excitation at 355 nm NADH forms solvated electrons as well as radical species (53, 54), which can then reduce the T1Cu either directly or through mediation by a radical species of NMN (23). In Fig. 3, typical absorbance changes are presented as recorded during the laser experiments. In the absence of substrate (Fig. 3, *A* and *C*), the *Ax*NiR enzyme with fully reconstituted copper centers showed the expected decrease in absorbance upon T1Cu reduction, which was followed by a subsequent partial recovery of the absorbance signal, reporting on T1- to T2Cu ET. The traces were analyzed double exponentially (Equation 3) with a first-order reduction rate ($k_{1(obs)}$), which did not depend on the NADH concentration between 50 and 250 μM and was ~10 times faster than the second observed rate constant (supplemental Fig. S5, *C* and *D*). The concentration independence of the reduction rate indicates that the observed process cannot be described by a simple bimolecular collision event, because this would be expected to yield

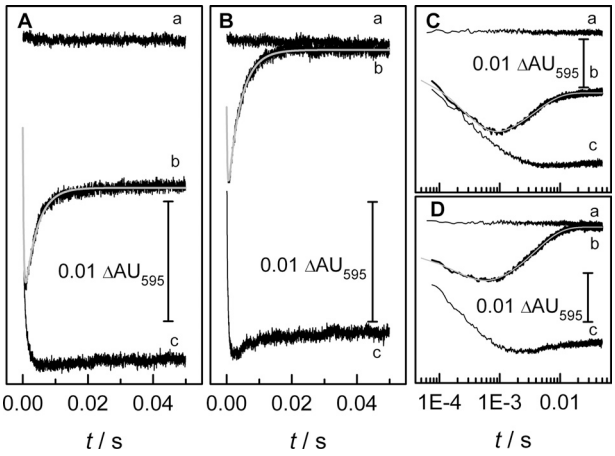

FIGURE 3. **Absorbance changes at 595 nm observed in the laser instrument upon reducing NiR and T2DNiR with NADH (λ_{exc} = 355 nm).** The sample mixture contained 200 μM NADH and 50 mM NMN in 50 mM KP_i, pH 7.0, at 4 °C. The *bars* reflect 0.01 ΔAU_{595}. *Traces* were slightly offset for clarity. *A* and *C, trace a,* control sample without enzyme; *trace b,* + 30 μM NiR; *trace c,* + 30 μM T2DNiR; *gray line*, double-exponential fit. *B* and *D,* as in *A* and *C* but in the presence of 10 mM KNO_2. Please note that the data sets shown in *A* (*B*) and *C* (*D*) are identical with the data in *A* (*B*) being presented on a linear time scale and the data in *C* (*D*) being plotted logarithmically to allow a reasonable demonstration of both the differences between the traces and the fits.

a linear dependence on the active electron concentration (55). Rather, the reduction of the T1Cu appears to be rate-limited by another reaction step, such as a conformational change. The absorbance changes at 595 nm (ΔAU_{595}) were not significantly dependent on the NADH concentration either. Using the mediator NMN did not change the reduction rates but increased the efficiency by about 30% (*i.e.* yielded larger ΔAU_{595}). The second observed rate constant ($k_{2(obs)}$) was ~370 s^{-1} at 4 °C and pH 7.0. This rate constant has contributions from at least the sum of $k_{2(forward)}$ and $k_{2(reverse)}$ (7, 20, 30), but it may well include further reaction steps coupled to the monitored ET signal (see below).

When T2DNiR, NiR lacking the copper atom in the T2Cu center (27, 42, 44), was used in these experiments, only the down-phase could be detected, thus substantiating that the up-phase, corresponding to $k_{2(obs)}$, actually reports on inter-copper ET and not on any other oxidation event of the T1Cu. With 10 mM nitrite present, however, the T2D enzyme did show a slight recovery of the AU_{595} signal subsequent to reduction, which can be explained by the presence of ~10% residual T2Cu typically found in T2D preparations of the enzyme (11, 14, 37). Alternatively, it has been demonstrated previously that "unmetallated" NiR exhibits some residual catalytic activity (7, 16, 22, 42, 43), which may also explain the slight recovery of the AU_{595} signal. Because crystal structures did not reveal any interaction of NO_2^- with the T1Cu center (14, 27), the substrate has been suggested to bind to the unmetallated T2Cu center (22). Similar apparent steady-state affinities were measured for T2D and native *Axg*NiR, which was accounted for by the retained hydrogen bonding network in the active site (8, 22). The nitrite reduction activity of T2D-*Axg*NiR was found to constitute ~10% of the native steady-state rate (22), which would be in accordance with both the presence of 10% fully copper-bound NiR and 10% residual activity of unmetallated T2Cu. Comparing our sample spectra before and after the laser experiment provided further indications that catalytic turnover can possibly take place in the T2DNiR sample (supplemental Fig. S5). Although both *Ax*NiR and T2D-*Ax*NiR remained partially reduced after photoexcitation in the absence of substrate, the absorbance spectra of both enzyme species were not significantly changed in the presence of nitrite, indicating complete re-oxidation and hence product formation in both cases.

Substrate Concentration Dependence, SKIE, and Proton Inventory Experiments in Pre-steady State—Analogous to the steady-state deoxyHb assay, laser experiments were performed using 50 mM KP_i in 100% H_2O, pH 7.0, and in 95% D_2O, pD 7.0, as solvent (Fig. 4, *A–D*, and supplemental Fig. S6). In the absence of nitrite, a SKIE of 1.43 ± 0.06 was obtained (Fig. 4, *E* and *F*), a SKIE similar to the steady-state (k_{cat}) SKIE value of 1.3 ± 0.1 (Fig. 2). The detection of a SKIE in the absence of substrate indicates that the inter-copper ET is linked to a PT step irrespective of the chemical conversion of nitrite (see Scheme 2, reaction sequence 1). This link between the inter-copper ET and a PT step may be explicable by several scenarios as follows: (i) a stepwise transfer of a proton and an electron exhibiting a kinetic gating mechanism, in which a slow PT step preceding ET rate-limits the observed ET process (56, 57); (ii) a stepwise mechanism, in which a thermodynamically unfavorable yet fast PT pre-equilibrium results in a decrease in the observed ET rate constant (kinetically coupled ET (56, 57)); or (iii) a concerted transfer of both proton and electron in a single elementary reaction (58, 59). Please note that in this study all these options are captured by the expression proton-coupled electron transfer, although a manifold of definitions can be found for the term proton-coupled electron transfer in the literature (for example see Refs. 58–66).

The substrate concentration dependences of the observed rate constants ($k_{2(obs)}$) were also determined in the laser experiments. In a previous publication (27) a random sequential mechanism has been suggested, in which nitrite binds preferentially to the enzyme species with a reduced T1Cu center and an oxidized T2Cu center but is also able to bind to the fully oxidized NiR at elevated concentrations. For the presented laser experiments, it can therefore be assumed that a pre-equilibrium between substrate-free and nitrite-bound oxidized *Ax*NiR exists prior to the laser flash (Scheme 2, *gray box*). The equilibrium position is a function of the nitrite concentration present in the sample and may include the first protonation event (see Scheme 1). Consequently, the T1Cu centers of both the substrate-free and the nitrite-bound enzyme species can be reduced by the electron donor upon photoexcitation. An additional reaction branching may be obtained subsequent to the T1Cu reduction by binding of nitrite to the T2Cu center of *Ax*NiR. This reaction step may also include a PT process. According to Ref. 27, the substrate affinity of the T1Cu-reduced enzyme species is greater than that of the completely oxidized enzyme. The inter-copper ET observed in the presence of nitrite may therefore include varying contributions from all three reaction sequences labeled 1–3 in Scheme 2 depending on the

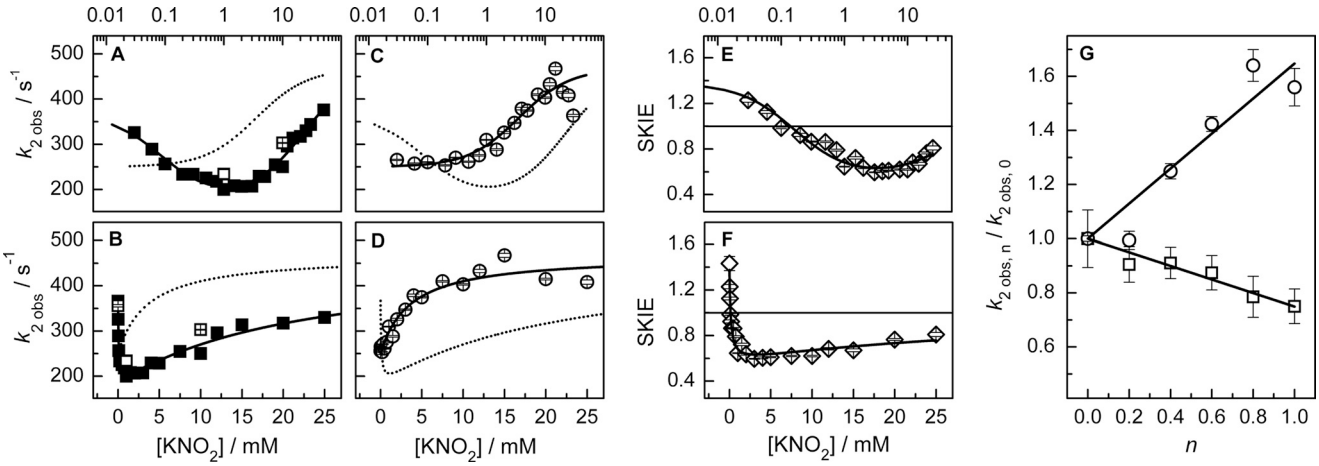

FIGURE 4. **Effect of the substrate concentration dependence on the observed rate constant $k_{2(obs)}$ measured at 4 °C in laser photoexcitation experiments.** The reaction mixture contained 30 μM NiR, 200 μM NADH. and 50 mM NMN in 50 mM KP_i. In a control experiment, the total ionic strength was adjusted to [KNO_2] + [KCl] = 50 mM (*open squares* in *A* and *B*), to ascertain that the changing ion concentration upon titration of nitrite was negligible. The *error bars* are smaller than the symbol size if invisible. *A* and *B, closed squares,* 100% H_2O, pH 7.0; *open squares,* data obtained in 100% H_2O with an ionic strength of [KNO_2] + [KCl] = 50 mM; *solid lines*, fit to an equation reflecting two substrate-binding sites (Equation 7, 100% H_2O, pH 7.0); *dotted lines*, fit to D_2O data set shown in *C* and *D*. *C* and *D, open circles*, 95% D_2O, pD 7.0; *solid lines,* fit to a hyperbolic equation (95% D_2O, pD 7.0, Equation 6); *dotted lines*, fit to H_2O data set shown in *A* and *B*. *E* and *F,* substrate concentration dependence of the SKIE obtained as the ratio of the observed rate constants $k_{2(obs)}$ in H_2O and D_2O. The *solid line* represents a fit to a simplified equation reflecting two substrate-binding sites (Equation 8). *G,* proton inventory plots. The ratio of the observed rate constant $k_{2(obs)rn}$, obtained at a certain volume fraction of D_2O(*n*), and the rate constant $k_{2(obs),\,0}$ in pure H_2O is plotted *versus n*. The pH values of D_2O-containing buffers were adjusted according to Equation 1. *Squares*, substrate-free sample; *circles*, sample mixture including 10 mM KNO_2. The *solid lines* are fits to Equation 4. Please note that the data sets presented in *A* and *B* (*C* and *D*; *E* and *F*) are identical. The data in *A* (*C*; *E*) are plotted logarithmically over the complete concentration range, whereas the data in *B* (*D*; *F*) are shown over a linear concentration range. To ensure the recognizability of the behavior at lower substrate concentrations on the linear scale (*B*; *D*), the presented concentration range is slightly smaller than on the logarithmic plot (*A*; *C*).

substrate concentration[5] (14, 16, 19, 26, 27, 33, 46). For several reasons this mechanism is difficult to model mathematically: (i) there may be a pre-equilibrium yielding (at least) two initial enzyme species; (ii) laser experiments are treated as equilibrium perturbation experiments (7, 20, 30) resulting in complex expressions for multistep reactions (67); (iii) reaction branching is likely to occur after the T1Cu reduction, *i.e.* after equilibrium perturbation, necessitating even more intricate mathematic expressions. This theoretically expected intricacy was mirrored in the complex kinetic behavior observed. In the following paragraphs, the significantly different substrate concentration dependences found for the $k_{2(obs)}$ values in H_2O and D_2O will be discussed.

The substrate concentration dependence in D_2O (Fig. 4, *C* and *D*) resembles an offset hyperbolic equation and could be analyzed by Equation 6,

$$k_{2(obs)} = k_{2(zero)} + \frac{dk_{2(obs)} \cdot [KNO_2]}{K_{s(app)} + [KNO_2]} \qquad \text{(Eq. 6)}$$

yielding an apparent saturation constant ($K_{s(app)}$), an observed rate constant $k_{2(zero)}$ in the absence of substrate and an observed difference rate constant $dk_{2(obs)}$ (Table 1). If the monitored inter-copper ET merely functioned as a reporter reaction of a simple bimolecular binding event, a linear concentration dependence would be expected. Hyperbolic concentration dependences, however, are frequently observed in enzymatic

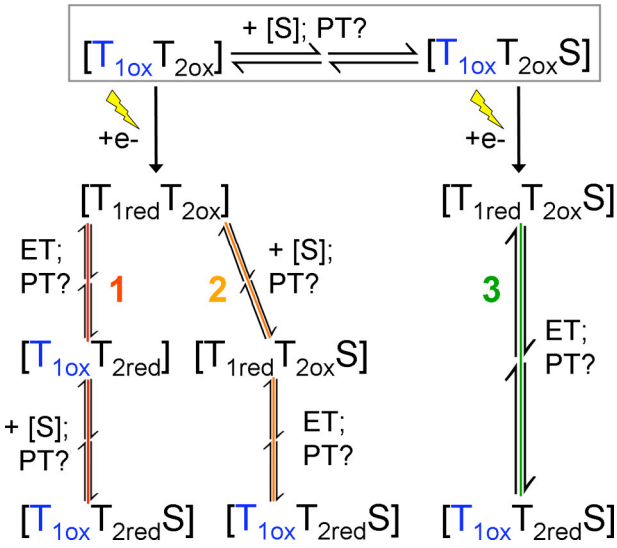

SCHEME 2. **Random mechanism suggested for NiR (27).** $T_{1(ox)}$, oxidized blue T1Cu; $T_{1(red)}$, reduced colorless T1Cu; $T_{2(ox)}$, oxidized T2Cu; $T_{2(red)}$, reduced T2Cu: *S*, substrate; e^-, electron. The *gray box* symbolizes the pre-equilibrium likely to exist prior to photoexcitation (*yellow arrow*) in the laser experiments. Please note that the order of the reaction steps labeled "*x*; *y*" is unknown and that all reaction steps may be concerted rather than sequential as suggested by the *arrows*. The ET reaction may also be coupled to subsequent PT steps. See text for further explanation.

systems (55) and are indicative of another reaction step being reflected in the observed rate constant, such as a slow step following substrate binding or an activation step prior to substrate binding (55) (see supplemental material for further information). The actual kinetic mechanism in *Ax*NiR leading to the hyperbolic behavior may be much more complicated. The presented case of *Ax*NiR is complicated by the fact that the observed inter-copper ET can also take place in the substrate-

[5] For *Af*NiR (*Alcaligenes faecalis* S-6), a random-sequential mechanism has been postulated, in which the inter-copper ET precedes substrate binding at low nitrite concentrations but follows it at high nitrite concentrations (46). This suggestion, however, contradicts other findings indicating an inactivation of NiR with a prematurely reduced T2Cu center (14, 16, 19, 26, 27, 33).

TABLE 1

Substrate concentration dependence of the observed T1- to T2Cu ET process in AxNiR

The parameters obtained from the fits to Equations 6–8 are listed.

H_2O (Eq. 7)						
	ΔAU_{zero}	$d\Delta AU_{2(obs)1}$	$d\Delta AU_{2(obs)2}$	$K_{s(app)1}$, mM	$K_{s(app)2}$, mM	R^2
$\Delta AU_{2(obs)}$	0.010 ± 0.001	0.014 ± 0.0016	-0.016 ± 0.006	0.03 ± 0.01	31 ± 12	0.9443
	k_{2zero}, s^{-1}	$dk_{2(obs)1}$, s^{-1}	$dk_{2(obs)2}$, s^{-1}	$K_{s(app)1}$, mM	$K_{s(app)2}$, mM	R^2
$k_{2(obs)}$, s^{-1}	367 ± 9	-188 ± 10	99 ± 30	0.088 ± 0.018	22 ± 5	0.9746

D_2O (Eq. 6)						
	k_{2zero}, s^{-1}	$dk_{2(obs)}$, s^{-1}		$K_{s(app)}$, mM		R^2
$k_{2(obs)}$, s^{-1}	250.0 ± 7.7	217.5 ± 16.1		3.6 ± 1.0		0.9455

SKIE (Eq. 8)						
	$SKIE_{zero}$	dSKIE		$K_{s(app)1}$, mM	$K_{s(app)2}$, mM	R^2
SKIE	1.24 ± 0.05	-0.83 ± 0.07		0.46 ± 0.16	23 ± 8	0.9239

free enzyme on a comparable time scale. This reaction has been accounted for by the concentration-independent rate constant $k_{2(zero)}$. The partitioning between the two signal sources is reflected in Equation 6 by adding a concentration-dependent term with a difference rate constant $dk_{2(obs)}$. Consequently, the $k_{2(obs)}$ value equals $k_{2(zero)}$ in the absence of substrate, whereas $k_{2(obs)}$ is the sum of $k_{2(zero)}$ and the positive $dk_{2(obs)}$ value at saturating nitrite concentrations indicating accelerated inter-copper ET rates in the nitrite-bound enzyme.

In contrast to the behavior found in D_2O, the $k_{2(obs)}$ values in H_2O decreased upon addition of moderate substrate concentrations (up to ~10 mM) indicative of a decelerated observed inter-copper ET in the substrate-bound *Ax*NiR. This is in accordance with previously published pulse radiolysis data (7, 19–22) and contravenes the proposed change in the driving force upon substrate binding (see Introduction and Refs. 7, 16, 23, 25, 27–30). At more elevated nitrite concentrations, however, the inter-copper ET rates approached the values in the absence of substrate. Therefore, this unusual behavior could not be analyzed by a modified hyperbolic expression. Phenomenologically, the observed behavior resembles substrate inhibition-type patterns found in steady-state kinetics, in which an increase in the rate constant occurs at moderate substrate concentrations followed by a subsequent decrease at higher amounts (68–70). In the presented case, however, the inverse effect is reflected in Fig. 4, *A* and *B*, with the addition of moderate substrate concentrations leading to an observed decrease in $k_{2(obs)}$ and an increase at very high concentrations. In the absence of any obvious mechanism accounting for the differential behaviors found in the two solvents, a phenomenological analysis of the H_2O data set still allows comparison of the curvatures characterizing the decreasing and increasing sections (Fig. 4, *A* and *B*) with the $K_{s(app)}$ value obtained for the D_2O data set (Fig. 4, *C* and *D*; Table 1). Therefore, an equation accounting for two apparent substrate-binding sites adapted from steady-state inhibition schemes was employed for the H_2O data[6] (Equation 7; see supplemental material for further information) (68–70).

$$k_{2(obs)} = k_{2(zero)} + \frac{dk_{2(obs)1} \cdot [KNO_2]/K_{s(app)1}}{a} + \frac{dk_{2(obs)2} \cdot [KNO_2]^2/(K_{s(app)1} \cdot K_{s(app)2})}{a} \quad \text{(Eq. 7)}$$

$$a = 1 + [KNO_2]/K_{s(app)1} + [KNO_2]/K_{s(app)2} + [KNO_2]^2/(K_{s(app)1} \cdot K_{s(app)2})$$

Equation 7 yields two apparent saturation constants, one of apparent high affinity ($K_{s(app)1}$) and the other of apparent low affinity ($K_{s(app)2}$), as well as two difference rate constants ($dk_{2(obs)1}$, $dk_{2(obs)2}$). The apparent saturation constants are phenomenological values and should be treated only qualitatively. A reasonable fit with $K_{s(app)}$ values of ~0.088 ± 0.018 and 22 ± 5 mM was obtained in comparison with the single $K_{s(app)}$ of 3.6 ± 0.9 mM in 95% D_2O (Table 1). Whereas $dk_{2(obs)1}$ is negative reflecting the initial decrease in Fig. 4, *A* and *B*, $dk_{2(obs)2}$ is a positive value accounting for the increase in $k_{2(obs)}$ at high nitrite concentrations. It is noteworthy that the $\Delta AU_{2(obs),595}$ increased about 2-fold upon addition of moderate nitrite concentrations followed by a subsequent decrease (supplemental Fig. 6) and could therefore also be analyzed using an equation analogous to Equation 7 (Table 1). This observation may indicate that the thermodynamic equilibrium at moderate nitrite concentrations is driven toward the oxidized T1Cu (*i.e.* toward the product side of the reaction) as is expected from the suggested change in $\Delta E'_0$ upon substrate binding (see Introduction and Refs. 7, 16, 23, 25, 27–30). Alternatively, the improved kinetic resolution of the T1Cu reduction upon photoexcitation and the subsequent inter-copper ET might yield apparently enlarged amplitudes at moderate substrate concentrations.

Comparison of the observed inter-copper ET rates with the catalytic activity of *Ax*NiR at a certain substrate concentration reveals that the smallest ratio of pre-steady-state and steady-state rates was observed around 1 mM substrate. At this nitrite concentration the $k_{2(obs)}$ value is 3.3-fold faster than the catalytic rate constant in H_2O, whereas the corresponding rate constants in D_2O are separated by a factor as large as 6.5. This finding suggests that the events rate-limiting inter-copper ET are too fast to be reflected in the steady-state SKIE. In other words, the proton involved in rate-limiting the steady-state turnover is unlikely to be identical with the PT step affecting the inter-copper ET observed in the transient kinetics. This conclusion is also emphasized by the different substrate-concentration dependences of the SKIE in the steady-state and the laser experiments. Although a normal steady-state SKIE was obtained up to 50 mM nitrite (Fig. 2), an inverted SKIE was observed in the pre-steady-state above 0.1 mM nitrite (Fig. 4, *E* and *F*). The substrate concentration dependence of the pre-steady-state SKIE exhibits a trend similar to that for $k_{2(obs)}$ in H_2O and was analyzed using the simpler Equation 8, accounting for the SKIE in the absence of substrate ($SKIE_{(zero)}$) and two apparent substrate-binding sites (see supplemental material for further information),

[6] Please note that Equation 7 has been adapted from established equations (see supplemental material) and has not been derived for a particular mechanism in *Ax*NiR. The resulting values are therefore of phenomenological value only and cannot be assigned to defined reaction steps at this stage. Please treat these parameters only qualitatively.

$$SKIE_{obs} = SKIE_{zero} + \frac{dSKIE \cdot [KNO_2]}{K_{s(app)1} + [KNO_2] \cdot \left(1 + \frac{[KNO_2]}{K_{s(app)2}}\right)} \quad \text{(Eq. 8)}$$

The resulting values are given in Table 1.[7]

To substantiate the unusual behavior of the SKIE in the laser experiments, proton inventory experiments were conducted in the presence of 10 mM nitrite and in the absence of substrate (Fig. 4*G*). The normal SKIE behavior was confirmed for the substrate-free experiment, and a linear relationship between $k_{2(obs)}$ and the D_2O concentration was observed. This linearity is indicative of one solvent-exchangeable proton or one solvent molecule being involved in rate-limiting the observed inter-copper ET irrespective of the chemical conversion of nitrite (see above and Ref. 47) The SKIE obtained from the linear fit (Equation 4) was 1.33 ± 0.05. A curved proton inventory plot, in contrast, would have suggested the contribution of more than one proton/one solvent molecule (47, 48). In the presence of 10 mM KNO_2 the unusual inverted SKIE was validated, yielding linearly increasing $k_{2(obs)}$ values upon addition of D_2O. The SKIE determined from the fit (Equation 4) was 0.61 ± 0.02, which circumstantiates the above findings that ET in the substrate-bound *Ax*NiR is apparently accelerated in D_2O compared with H_2O.

Despite the significantly different trends in H_2O and D_2O and the reasonable fit results, limited experimental evidence is available to support the use of Equation 7 and 8, which assume two apparent substrate-binding sites. Unspecific, *i.e.* non-T2Cu-related, nitrite binding has actually been reported (37) and might account for an allosteric behavior in NiR, but there are no reports allocating the second binding site or attributing any effects on the enzymatic activity. The possibility that nitrite can bind to the T1Cu center has been excluded (32), and no competitive binding of two substrate molecules within the active site has been observed so far (46).

The actual reasons for the unusual substrate concentration dependence in H_2O and the observed inverted SKIE remain elusive. Both findings, however, may be explicable by a complex mechanism, which includes parallel reaction pathways and branching points analogous to that suggested in Scheme 2. The observation of inverted SKIEs has previously been attributed to reaction branching or to a PT step with a solvent-dependent equilibrium constant (71–73). The unusual substrate concentration dependence in H_2O may also result from the differential population of various pathways governed by the nitrite concentration. Irrespective of the kinetic mechanism forming the basis of the unusual data, the contrasting behavior of $k_{2(obs)}$ in H_2O and D_2O is evident, and the significant SKIE provides strong evidence that inter-copper ET in *Ax*NiR is proton-coupled.

Temperature Dependence of Inter-copper ET—One of the crucial differences between crystallographic and solution studies on NiR concerns the occurrence of inter-copper ET in the absence of substrate. Although inter-copper ET in substrate-free NiR can be observed in pulse radiolysis (7, 19–22) as well as in our laser photoexcitation experiments, the equilibration of electrons between the T1Cu and T2Cu in the protein crystal could only be established in the presence of substrate (34). At 4 °C and pH 7.0, our studies in the solvent H_2O suggested that inter-copper ET is actually faster in the absence of substrate. The crystal studies, however, were conducted by preferentially reducing the T1Cu center of NiR with the x-ray beam, whereas a nitrogen cryostream was used to cool the sample to 100 K to diminish the destructive effect of the x-ray radiation. Thus, a direct comparison between our solution experiments at 4 °C and the crystal studies at 100 K is not possible without extrapolating the influence of the temperature on the observed ET rates. Therefore, we measured the temperature dependence of the $k_{2(obs)}$ values in the absence of substrate and in the presence of moderate nitrite concentrations (10 mM) between 4 and 40 °C (Fig. 5). The data were analyzed using the Eyring (Equation 5) and the Marcus equation (see supplemental Table S1 and supplemental Fig. S7) (74). The Marcus analysis did not allow us to conclude whether ET is gated, *i.e.* kinetically rate-limited by a slow reaction step such as PT, which would be expected to result in unreasonable Marcus parameters (see supplemental material). A stepwise, kinetically coupled PCET (see definition above), however, may still give reasonable Marcus parameters, which are not necessarily in disagreement with a true ET (74). In concerted PCET reactions, both proton and electron tunnel synchronously,[8] and special mathematical expressions (59, 75–85) are needed to account for the kinetic and thermodynamic mutual influence exerted by the two moving charges (86). As the transition state of a concerted transfer can either be more ET-like or more PT-like (59), the Marcus parameters resulting from a concerted PCET reaction may or may not be in accordance with the expectation values for a true ET. With the isotope studies presented above clearly indicating

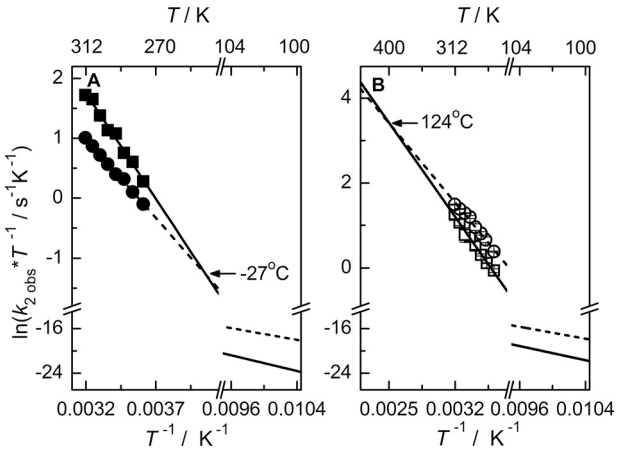

FIGURE 5. **Temperature dependences for the observed rate constants $k_{2(obs)}$ measured in laser photoexcitation experiments.** *Squares,* substrate-free sample containing 30 μM NiR; *circles*, 30 μM NiR + 10 mM KNO_2. *Lines* are extrapolated fits to the Eyring equation (Equation 5). *Solid lines*, substrate-free; *dashed lines*, + 10 mM KNO_2. *A,* 50 mM KP_i in 100% H_2O, pH 7.0. *B,* 50 mM KP_i in 95% D_2O, pD 7.0.

[7] Because of the limited number of data points, Equation 7 did not converge for $K_{s(obs)2}$. As discussed in Footnote 6, the physical meaning of the obtained parameters is elusive, and the phenomenology of the observed behavior is well captured by the employed mathematical analysis.

[8] Please note that synchronously is not synonymous for simultaneously but that simultaneous PCET is a special case of concerted PCET.

TABLE 2

Temperature dependencies of the observed inter-Cu ET process in AxNiR

The activation parameters resulting from the Eyring fits (Eq. 5) are shown. The experiment was performed in 50 mM KP_i, pH 7.0 (100% H_2O), and pD 7.0 (95% D_2O).

	$\Delta H^{\ddagger}$	$\Delta S^{\ddagger}$	$\Delta G^{\ddagger}$ (298 K)	*R*^2
	kJ/mol	*kJ/(mol·K)*	*kJ/mol*	
H_2O, substrate-free	29.3 ± 1.3	−0.089 ± 0.004	55.9 ± 2.6	0.9885
D_2O, substrate-free	26.4 ± 1.2	−0.103 ± 0.004	57.1 ± 2.4	0.9884
H_2O + 10 mM KNO_2	22.0 ± 0.5	−0.119 ± 0.002	57.4 ± 1.0	0.9968
D_2O + 10 mM KNO_2	22.4 ± 1.0	−0.113 ± 0.004	56.1 ± 2.1	0.9874

a PCET, the conclusion suggests itself that the observed PCET events in *Ax*NiR are either because of a kinetically coupled, stepwise transfer of a proton and an electron or result from a concerted transfer of the two charges in a single elementary reaction step. The activation parameters obtained in the Eyring analysis were similar to those published in pulse radiolysis studies (Table 2) (19, 20, 30). The activation enthalpies were found to be smaller in the presence of substrate, whereas the activation entropies are less favorable than in the absence of substrate. Thus, the balance of $\Delta S^{\ddagger}$ and $\Delta H^{\ddagger}$ determines whether the observed reaction is faster in the absence of substrate (as found in H_2O) or in the presence of nitrite (as observed in D_2O). The linear Eyring fits were extrapolated to lower temperatures, assuming the absence of a break point (Fig. 5). For the H_2O data sets, the substrate-free and nitrite-bound linear regressions were found to have an intersection point at −27 °C. This crossover suggests that inter-copper ET below this temperature becomes increasingly attenuated for the substrate-free enzyme in comparison with the nitrite-bound enzyme species. The extrapolation also allows a rough estimate of $k_{2(obs)}$ under the conditions used in the crystallographic studies (34). At 100 K, the resulting inter-copper ET rates are 2×10^{-8} s^{-1} in the absence of substrate and 3×10^{-6} s^{-1} at 10 mM nitrite, *i.e.* the rate of ET was calculated to be 150-fold faster in the presence of substrate. This separation is expected to be sufficient to allow the experimental observation of ET in the presence, but not in the absence, of substrate because the duration of the experiment was limited to ~8–17 min (34). In conclusion, our studies provide a possible explanation for the apparent discrepancy between solution and crystal studies.

Conclusions—Our present work on wild-type *Ax*NiR provided the first direct evidence that two protons are involved in the catalytic turnover at pH 7.0. A normal steady-state SKIE of 1.3 ± 0.1 was determined for nitrite concentrations up to 50 mM, indicating that one proton or one solvent molecule contributes to the rate-limiting step of the catalytic process. Single turnover experiments, monitoring the inter-copper ET, established a SKIE of ~1.33 ± 0.05 in the absence of substrate, which is indicative of a PCET irrespective of product formation. The substrate concentration dependence of the inter-copper ET revealed an apparently inverted SKIE at nitrite concentrations ≥0.1 mM, which is possibly a result of comparing differential populations of various reaction routes in H_2O and D_2O, in accordance with a random-sequential mechanism. The protonation events affecting the single and the multiple turnover experiments, respectively, are unlikely to originate from the same reaction step. Thus, both protons involved in the overall mechanism as shown by the phenol red experiments might be reflected in the presented kinetic data, one in the transient laser experiments and the other in the catalytic turnover of *Ax*NiR. Alternatively, the same proton might be involved in two different reaction steps, one affecting the catalytic turnover and one the transient kinetics. The temperature dependences of the ET provided a possible explanation for the seeming contradiction between crystallographic and solution data, concerning the coupling of ET to the presence of substrate. Further investigations will be required to establish whether structural changes upon binding of nitrite at the T2Cu site actually trigger the ET from the reduced T1Cu center.

REFERENCES

1. Averill, B. A. (1996) *Chem. Rev.* **96,** 2951–2964
2. Ichiki, H., Tanaka, Y., Mochizuki, K., Yoshimatsu, K., Sakurai, T., and Fujiwara, T. (2001) *J. Bacteriol.* **183,** 4149–4156
3. Zumft, W. G. (1997) *Microbiol. Mol. Biol. Rev.* **61,** 533–616
4. Baker, S. C., Saunders, N. F., Willis, A. C., Ferguson, S. J., Hajdu, J., and Fülöp, V. (1997) *J. Mol. Biol.* **269,** 440–455
5. Nurizzo, D., Silvestrini, M. C., Mathieu, M., Cutruzzolà, F., Bourgeois, D., Fülöp, V., Hajdu, J., Brunori, M., Tegoni, M., and Cambillau, C. (1997) *Structure* **5,** 1157–1171
6. Fülöp, V., Moir, J. W., Ferguson, S. J., and Hajdu, J. (1995) *Cell* **81,** 369–377
7. Suzuki, S., Kataoka, K., and Yamaguchi, K. (2000) *Acc. Chem. Res.* **33,** 728–735
8. Adman, E. T., Godden, J. W., and Turley, S. (1995) *J. Biol. Chem.* **270,** 27458–27474
9. Dodd, F. E., Van Beeumen, J., Eady, R. R., and Hasnain, S. S. (1998) *J. Mol. Biol.* **282,** 369–382
10. Kataoka, K., Yamaguchi, K., Kobayashi, M., Mori, T., Bokui, N., and Suzuki, S. (2004) *J. Biol. Chem.* **279,** 53374–53378
11. Howes, B. D., Abraham, Z. H., Lowe, D. J., Brüser, T., Eady, R. R., and Smith, B. E. (1994) *Biochemistry* **33,** 3171–3177
12. Dodd, F. E., Hasnain, S. S., Abraham, Z. H., Eady, R. R., and Smith, B. E. (1995) *Acta Crystallogr. D Biol. Crystallogr.* **51,** 1052–1064
13. Zumft, W. G., Gotzmann, D. J., and Kroneck, P. M. (1987) *Eur. J. Biochem.* **168,** 301–307
14. Strange, R. W., Dodd, F. E., Abraham, Z. H., Grossmann, J. G., Brüser, T., Eady, R. R., Smith, B. E., and Hasnain, S. S. (1995) *Nat. Struct. Biol.* **2,** 287–292
15. Antonyuk, S. V., Eady, R. R., Strange, R. W., and Hasnain, S. S. (2003) *Acta Crystallogr. D Biol. Crystallogr.* **59,** 835–842
16. Yousafzai, F. K., and Eady, R. R. (2002) *J. Biol. Chem.* **277,** 34067–34073
17. Dodd, F. E., Hasnain, S. S., Abraham, Z. H., Eady, R. R., and Smith, B. E. (1997) *Acta Crystallogr. D Biol. Crystallogr.* **53,** 406–418
18. Ellis, M. J., Prudêncio, M., Dodd, F. E., Strange, R. W., Sawers, G., Eady, R. R., and Hasnain, S. S. (2002) *J. Mol. Biol.* **316,** 51–64
19. Farver, O., Eady, R. R., Sawers, G., Prudêncio, M., and Pecht, I. (2004) *FEBS Lett.* **561,** 173–176
20. Farver, O., Eady, R. R., Abraham, Z. H., and Pecht, I. (1998) *FEBS Lett.* **436,** 239–242
21. Kobayashi, K., Tagawa, S., Deligeer, and Suzuki, S. (1999) *J. Biochem.* **126,** 408–412
22. Kataoka, K., Furusawa, H., Takagi, K., Yamaguchi, K., and Suzuki, S. (2000) *J. Biochem.* **127,** 345–350
23. Suzuki, S., Deligeer, Yamaguchi, K., Kataoka, K., Kobayashi, K., Tagawa, S., Kohzuma, T., Shidara, S., and Iwasaki, H. (1997) *J. Biol. Inorg. Chem.* **2,** 265–274
24. Suzuki, S., Kataoka, K., Yamaguchi, K., Inoue, T., and Kai, Y. (1999) *Coord. Chem. Rev.* **190,** 245–265
25. Marcus, R. A., and Sutin, N. (1985) *Biochim. Biophys. Acta* **811,** 265–322
26. Wijma, H. J., Jeuken, L. J., Verbeet, M. P., Armstrong, F. A., and Canters, G. W. (2007) *J. Am. Chem. Soc.* **129,** 8557–8565
27. Strange, R. W., Murphy, L. M., Dodd, F. E., Abraham, Z. H., Eady, R. R., Smith, B. E., and Hasnain, S. S. (1999) *J. Mol. Biol.* **287,** 1001–1009

28. Antonyuk, S. V., Strange, R. W., Sawers, G., Eady, R. R., and Hasnain, S. S. (2005) *Proc. Natl. Acad. Sci. U.S.A.* **102,** 12041–12046
29. Hough, M. A., Ellis, M. J., Antonyuk, S., Strange, R. W., Sawers, G., Eady, R. R., and Samar Hasnain, S. (2005) *J. Mol. Biol.* **350,** 300–309
30. Wherland, S., Farver, O., and Pecht, I. (2005) *ChemPhysChem* **6,** 805–812
31. Kuznetsova, S., Zauner, G., Aartsma, T. J., Engelkamp, H., Hatzakis, N., Rowan, A. E., Nolte, R. J., Christianen, P. C., and Canters, G. W. (2008) *Proc. Natl. Acad. Sci. U.S.A.* **105,** 3250–3255
32. Kohzuma, T., Kikuchi, M., Horikoshi, N., Nagatomo, S., Kitagawa, T., and Czernuszewicz, R. S. (2006) *Inorg. Chem.* **45,** 8474–8476
33. Prudêncio, M., Sawers, G., Fairhurst, S. A., Yousafzai, F. K., and Eady, R. R. (2002) *Biochemistry* **41,** 3430–3438
34. Hough, M. A., Antonyuk, S. V., Strange, R. W., Eady, R. R., and Hasnain, S. S. (2008) *J. Mol. Biol.* **378,** 353–361
35. De Marothy, S. A., Blomberg, M. R., and Siegbahn, P. E. (2007) *J. Comput. Chem.* **28,** 528–539
36. Sundararajan, M., Hillier, I. H., and Burton, N. A. (2007) *J. Phys. Chem. B* **111,** 5511–5517
37. Abraham, Z. H., Smith, B. E., Howes, B. D., Lowe, D. J., and Eady, R. R. (1997) *Biochem. J.* **324,** 511–516
38. MacPherson, I. S., and Murphy, M. E. (2007) *Cell. Mol. Life Sci.* **64,** 2887–2899
39. Ellis, M. J., Dodd, F. E., Strange, R. W., Prudêncio, M., Sawers, G., Eady, R. R., and Hasnain, S. S. (2001) *Acta Crystallogr. D Biol. Crystallogr.* **57,** 1110–1118
40. Ghosh, S., Dey, A., Usov, O. M., Sun, Y., Grigoryants, V. M., Scholes, C. P., and Solomon, E. I. (2007) *J. Am. Chem. Soc.* **129,** 10310–10311
41. Ghosh, S., Dey, A., Sun, Y., Scholes, C. P., and Solomon, E. I. (2009) *J. Am. Chem. Soc.* **131,** 277–288
42. Harris, R. L., Prudêncio, M., Hasnain, S. S., Eady, R. R., and Sawers, R. G. (2005) *J. Synchrotron Radiat.* **12,** 13–18
43. Prudêncio, M., Eady, R. R., and Sawers, G. (1999) *J. Bacteriol.* **181,** 2323–2329
44. Abraham, Z. H., Lowe, D. J., and Smith, B. E. (1993) *Biochem. J.* **295,** 587–593
45. Burkhard, O., and Barnikol, W. K. (1982) *J. Appl. Physiol.* **52,** 124–130
46. Wijma, H. J., Jeuken, L. J., Verbeet, M. P., Armstrong, F. A., and Canters, G. W. (2006) *J. Biol. Chem.* **281,** 16340–16346
47. Schowen, K. B., and Schowen, R. L. (1982) *Methods Enzymol.* **87,** 551–606
48. Karpefors, M., Adelroth, P., and Brzezinski, P. (2000) *Biochemistry* **39,** 5045–5050
49. Wijma, H. J., Canters, G. W., de Vries, S., and Verbeet, M. P. (2004) *Biochemistry* **43,** 10467–10474
50. Moore, E. G., and Gibson, Q. H. (1976) *J. Biol. Chem.* **251,** 2788–2794
51. Dejam, A., Hunter, C. J., Schechter, A. N., and Gladwin, M. T. (2004) *Blood Cells Mol. Dis.* **32,** 423–429
52. Zhao, Y., Lukoyanov, D. A., Toropov, Y. V., Wu, K., Shapleigh, J. P., and Scholes, C. P. (2002) *Biochemistry* **41,** 7464–7474
53. Orii, Y. (1993) *Biochemistry* **32,** 11910–11914
54. Orii, Y., Miki, T., and Kakinuma, K. (1995) *Photochem. Photobiol.* **61,** 261–268
55. Strickland, S., Palmer, G., and Massey, V. (1975) *J. Biol. Chem.* **250,** 4048–4052
56. Davidson, V. L. (2000) *Acc. Chem. Res.* **33,** 87–93
57. Davidson, V. L. (2002) *Biochemistry* **41,** 14633–14636
58. Reece, S. Y., Hodgkiss, J. M., Stubbe, J., and Nocera, D. G. (2006) *Philos. Trans. R. Soc. Lond. B Biol. Sci.* **361,** 1351–1364
59. Reece, S. Y., and Nocera, D. G. (2009) *Annu. Rev. Biochem.* **78,** 673–699
60. Mayer, J. M. (2004) *Annu Rev. Phys. Chem.* **55,** 363–390
61. Chen, K., Hirst, J., Camba, R., Bonagura, C. A., Stout, C. D., Burgess, B. K., and Armstrong, F. A. (2000) *Nature* **405,** 814–817
62. Costentin, C. (2008) *Chem. Rev.* **108,** 2145–2179
63. Costentin, C., Evans, D. H., Robert, M., Savéant, J. M., and Singh, P. S. (2005) *J. Am. Chem. Soc.* **127,** 12490–12491
64. Graige, M. S., Paddock, M. L., Feher, G., and Okamura, M. Y. (1999) *Biochemistry* **38,** 11465–11473
65. Rappaport, F., and Lavergne, J. (2001) *Biochim. Biophys. Acta* **1503,** 246–259
66. Weatherly, S. C., Yang, I. V., Armistead, P. A., and Thorp, H. H. (2003) *J. Phys. Chem. B* **107,** 372–378
67. Bernasconi, C. F. (1976) *Relaxation Kinetics*, Academic Press, New York
68. Segel, I. H. (1975) *Enzyme Kinetics: Behavior and Analysis of Rapid Equilibrium and Steady-state Enzyme Systems*, Wiley-Interscience, New York
69. Bisswanger, H. (2008) *Enzyme Kinetics: Principles and Methods*, 2nd Ed., Wiley-VCH, New York
70. Leskovac, V. (2003) *Comprehensive Enzyme Kinetics*, Springer Inc., New York
71. Keeffe, J. R., and Jencks, W. P. (1981) *J. Am. Chem. Soc.* **103,** 2457–2459
72. Thibblin, A., and Ahlberg, P. (1989) *Chem. Soc. Rev.* **18,** 209–224
73. Northrop, D. B. (1981) *Annu. Rev. Biochem.* **50,** 103–131
74. Davidson, V. L. (2004) *Arch. Biochem. Biophys.* **428,** 32–40
75. Cukier, R. I. (2004) *Biochim. Biophys. Acta* **1655,** 37–44
76. Cukier, R. I. (1995) *J. Phys. Chem.* **99,** 16101–16115
77. Cukier, R. I. (1994) *J. Phys. Chem.* **98,** 2377–2381
78. Cukier, R. I. (2002) *J. Phys. Chem. B* **106,** 1746–1757
79. Cukier, R. I. (1996) *J. Phys. Chem.* **100,** 15428–15443
80. Cukier, R. I. (1999) *J. Phys. Chem. A* **103,** 5989–5995
81. Cukier, R. I., and Nocera, D. G. (1998) *Annu Rev. Phys. Chem.* **49,** 337–369
82. Hammes-Schiffer, S. (2001) *Acc. Chem. Res.* **34,** 273–281
83. Hammes-Schiffer, S. (2002) *ChemPhysChem* **3,** 33–42
84. Hammes-Schiffer, S., and Iordanova, N. (2004) *Biochim. Biophys. Acta* **1655,** 29–36
85. Hammes-Schiffer, S., and Soudackov, A. V. (2008) *J. Phys. Chem. B* **112,** 14108–14123
86. Stubbe, J., Nocera, D. G., Yee, C. S., and Chang, M. C. (2003) *Chem. Rev.* **103,** 2167–2201